

RESEARCH ARTICLE



Cite this: *Mater. Chem. Front.*,
2022, 6, 3422

Growth, structure and templating of anthradithiophene and its β -methylthiolated derivative

Chengyuan Wang,^{id}*^a Nadine Russegger,^a Giuliano Duva,^{†a}
Oleg V. Konovalov,^{id}^b Maciej Jankowski,^b Alexander Gerlach,^{id}^{ac}
Alexander Hinderhofer*^{ac} and Frank Schreiber^{id}*^{ac}

Organic semiconductor thin films are one of the key components in organic optoelectronics, and their structure, crystallinity, and morphology can significantly influence the properties and performance of the devices that they are used in. The thin film growth behavior of organic semiconductors can be affected by the molecular shape, substituents, growth conditions, and so on. Thus, understanding the growth mechanism and controlling the growth process is challenging, but crucially important. In this work, the thin film growth behaviors of two prototypical organic semiconductors, anthradithiophene (ADT) and its β -methylthiolated derivative (β -MT-ADT), which both have the same molecular backbone, with minor differences, in the substituents, but very different solid-state structures, *i.e.*, herringbone for ADT and rubrene-like “pitched” π -stacking for β -MT-ADT, were studied. The structure of the thin films was investigated using different X-ray diffraction (XRD) techniques, including X-ray reflectivity (XRR) for the out-of-plane structure, and synchrotron-based grazing-incidence wide-angle X-ray scattering (GIWAXS) for the in-plane structure. The morphologies of the thin films were explored with atomic force microscopy (AFM), and their thickness evolution was determined quantitatively within the dynamic scaling framework. In addition, the influence of substrate surface treatment on the thin film growth process of β -MT-ADT was studied using diindenoperylene (DIP) as the templating layer. This paper reports the thin film growth behaviors and structures of two representative organic semiconductors. It offers better understanding of the influence of minor molecular modifications on the thin film growth behavior, providing guidance for future material design and for developing high-performance organic semiconductors based on thin film structure design.

Received 27th July 2022,
Accepted 21st September 2022

DOI: 10.1039/d2qm00759b

rsc.li/frontiers-materials

Introduction

Organic semiconductors have been widely studied in the past decades for use in applications as organic light-emitting diodes (OLEDs), organic field-effect transistors (OFETs), organic photovoltaics (OPVs), and organic photodetectors due to their easy processability, low cost, flexibility, and so on.^{1–6} Thin films of organic semiconductors suitable for large-area and large-scale processing act as one of the key components in these

organic optoelectronics. The structure, crystallinity, and morphology of the organic semiconductor thin films can significantly influence the properties and performance of the devices.^{7–9} Therefore, understanding the growth mechanism and thus controlling the thin film growth process is important.^{10–12} At the same time, the physics of their growth is a serious fundamental challenge.¹³

Organic semiconductors are usually inherently anisotropic, so orientational degrees of freedom of the entire molecule as well as internal degrees of freedom (vibrations) have to be considered.^{14,15} Hence, their growth scenarios are more complex than those of conventional inorganic semiconductors. The molecular shape has proven to be an important factor affecting the thin film growth behavior, *e.g.*, for rod-like molecules such as pentacene or disk-like molecules such as metal phthalocyanines (MPc).^{16,17} Essentially the only exception is C₆₀, and similar fullerenes, with their (effectively) spherical shape and interaction potential.^{18,19} Therefore, the study of

^a Institute of Applied Physics, Universität Tübingen, Auf der Morgenstelle 10, 72076 Tübingen, Germany. E-mail: chengyuan.wang@ahu.edu.cn,

alexander.hinderhofer@uni-tuebingen.de, frank.schreiber@uni-tuebingen.de

^b ESRF–The European Synchrotron, 71 Avenue des Martyrs, CS 40220, 38043 Grenoble Cedex 9, France

^c Center for Light-Matter Interaction, Sensors & Analytics (LISA⁺), Universität Tübingen, Auf der Morgenstelle 15, 72076 Tübingen, Germany

[†] Current address: NMI-Naturwissenschaftliches und Medizinisches Institut, Markwiesenstraße 55, 72770 Reutlingen, Germany.

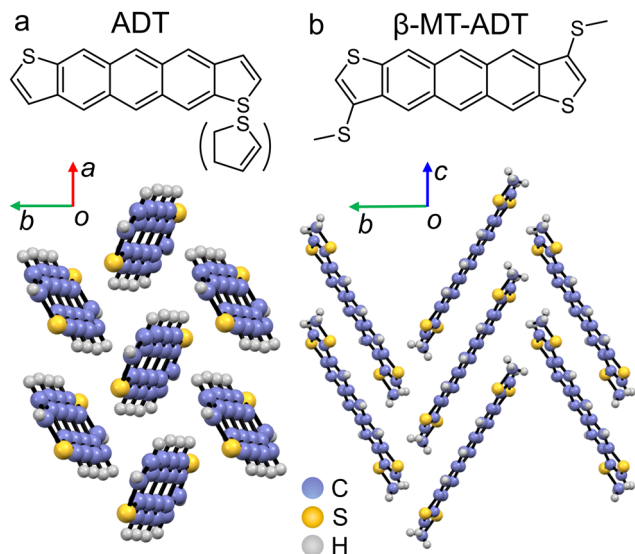


Fig. 1 Molecular and single-crystal structures of ADT³⁰ (a) and β -MT-ADT³¹ (b).

thin film growth mechanisms of organic semiconductors is a rather complex and challenging research field.²⁰

Furthermore, various substituents are often attached to the molecular backbone for tuning the molecular properties, which at the same time play significant roles in altering their thin film growth process.^{21–23} However, the thin film growth conditions, *e.g.*, substrate temperature, are vital for determining the structure and quality of the as-grown thin films.^{24,25} In particular, the surface treatment of the substrates can influence the thin film growth behavior in various ways, which is often discussed in terms of changing surface energies, organic–organic hetero-epitaxy, or templating effects.^{26–29}

Anthradithiophene (ADT) is a linear-shaped organic semiconductor with a molecular backbone resembling pentacene, with the difference being two carbon atoms being substituted by sulfur atoms at the ending rings (Fig. 1(a)). It has two isomers, *syn*-ADT and *anti*-ADT, which are difficult to separate during synthesis because of their similar chemical properties. As a result, ADT mixtures (containing *syn*- and *anti*-isomers in half/half ratio) are often used in organic optoelectronic devices, and mobilities above $1 \text{ cm}^2 \text{ V}^{-1} \text{ s}^{-1}$ have been achieved in thin film-based OFETs.^{32–34} Both the *syn*- and *anti*-isomers of ADT were reported to show a herringbone packing structure, similar to many prototypical rod-like organic semiconductors, whereas their unit cell parameters are slightly different.³⁰ Despite the abundant exploration of ADT, its thin film structure was so far mainly studied by standard X-ray diffraction (XRD) techniques based on out-of-plane structure characterization. The in-plane structure and the detailed growth behavior of ADT thin films have been rarely investigated. However, recently, a novel ADT derivative with its β -position modified by methylthio groups, namely β -MT-ADT, was reported (Fig. 1(b)). Intriguingly, the β -MT-ADT showed a rubrene-like “pitched” π -stacking structure in single crystals, which is strikingly different from the herringbone packing structure of the parent ADT and many

other prototypical rod-like organic semiconductors.³¹ This type of packing structure has only a few reported examples, and with this particular packing structure, its single-crystal-based OFETs reached mobilities up to $4.08 \text{ cm}^2 \text{ V}^{-1} \text{ s}^{-1}$ with SiO_2 as the dielectric layer. The performance was comparable to rubrene with a similar device structure, which is regarded as the best-performance p-type organic semiconductor in single-crystal OFETs.^{35,36} However, the thin film-based OFETs of β -MT-ADT only showed a mobility of $\sim 0.05 \text{ cm}^2 \text{ V}^{-1} \text{ s}^{-1}$ on the octadecyltrichlorosilane (ODTS) modified Si/SiO_2 substrate, which was almost two orders of magnitude lower than the single-crystal based ones. Because there was no detailed study on the thin film growth behavior of β -MT-ADT, it remains unclear why the thin film based devices showed such a large difference compared to the intrinsic charge transporting properties.

Considering the interesting characteristics of ADT and β -MT-ADT, *i.e.*, the same molecular backbone with minor differences in the substituents but a totally different packing structure in the solid state, and the lack of a detailed investigation of their thin film growth behavior, this work was dedicated to studying the growth and solid-state structures of ADT and β -MT-ADT thin films. Different XRD techniques, including X-ray reflectivity (XRR) and synchrotron-based grazing-incidence wide-angle X-ray scattering (GIWAXS), were utilized to determine the out-of-plane and in-plane structure of the thin films. Atomic force microscopy (AFM) was used to determine the morphology of the thin films, and their thickness evolution was studied quantitatively using a framework of dynamic scaling. In addition, the thin film growth process of β -MT-ADT on a diindenoperylene (DIP) layer was investigated to study how the surface treatment affected its thin film growth. This paper not only reports the thin film growth behaviors and structures of two interesting organic semiconductors, but also contributes to a better understanding of the influence of specific molecular functionalization on the growth behavior of thin films.

Experimental

The ADT, which was a mixture of *syn/anti* isomers with a mixing ratio of 50%, was purchased from Sigma-Aldrich and used directly without further purification. The β -MT-ADT synthesis was based on a procedure reported in the literature and purified by multiple sublimation processes.³¹ Thin films of ADT and β -MT-ADT were grown using organic molecular beam deposition (OMBD) under high-vacuum conditions (base pressure = 2×10^{-8} mbar).^{20,27,37} Native oxide silicon wafers ($\text{Si}(100)$) were used as substrates, which were cleaned in an ultrasonic bath with acetone and isopropanol, and heated to 500 K afterwards for degassing. During growth, the substrate temperature was kept at 300 K unless stated otherwise. The thin film growth rates were monitored with an SQM-160 quartz crystal microbalance (Inficon, Bad Ragaz, Switzerland), and were found to be 2 \AA min^{-1} for ADT and 8 \AA min^{-1} for β -MT-ADT. The surface morphology of the thin films was characterized by AFM

using a NanoWizard II (JPK Instruments, Berlin, Germany) in tapping mode. The XRR measurements were carried out on a XRD 3003 TT two-circle X-ray reflectometer (Seifert Analytical X-ray, Ahrensburg, Germany), with CuK α radiation, $\lambda = 1.54 \text{ \AA}$, and the critical angle was 0.12° for this wavelength. The values of q_z were calculated based on the equation $q = 4\pi(\sin\theta)/\lambda$, where θ is the incidence angle. The footprint correction was carried out for the XRR data. The GIWAXS characterization was conducted on the ID10 beamline (ESRF, France) with energy of 22 keV, $\lambda = 0.5636 \text{ \AA}$, and a Pilatus 300K 2D detector (Dectris, Baden-Daettwil, Switzerland). The incidence angle was 0.08° , and the data analysis was performed with Matlab software (MathsWorks, MA, USA).

Results and discussion

Out-of-plane structures of the thin films

The out-of-plane structures of ADT and β -MT-ADT thin films with different thicknesses were investigated by XRR (Fig. 2). One set of Bragg peaks with $q_z = 0.44n \text{ \AA}^{-1}$ ($n = 1, 2, 3$) were observed for ADT thin films when the nominal thickness was only 5 nm (Fig. 2(a)). The Bragg peaks essentially correspond to the (001) planes of *syn*-ADT and *anti*-ADT based on their single-crystal structures, respectively. As the thickness increased, the Bragg peaks became more pronounced. The out-of-plane lattice spacing (the distance between successive (*hkl*) planes) was calculated to be 14.28 \AA derived from the Bragg peak positions, which was very similar to the length of the ADT molecule (13.77 \AA , determined from the single-crystal structure). This suggested that ADT molecules grow uniaxially with an upright orientation on the substrate. In sharp contrast, no Bragg peaks were observed for the β -MT-ADT thin films, which indicated their low crystallinity.

In-plane structures of the thin films

To investigate the in-plane structures of ADT and β -MT-ADT thin films, GIWAXS experiments were conducted. Fig. 3(a) shows the corresponding reciprocal space map of an ADT thin

film with a 30 nm thickness, in which reflections can be observed with q_{xy} in the range of $1.2\text{--}2.2 \text{ \AA}^{-1}$. Based on the reciprocal space map, the unit cell parameters of the thin film were studied by fitting these reflections with the single-crystal structures of *syn*-ADT and *anti*-ADT, because the ADT used for thin film preparation was a mixture of the *syn*- and *anti*-isomers. The reflections roughly matched the single-crystal structure of *syn*-ADT with slight differences in the unit cell parameters (Table 1). The *a*-axis in the thin film showed a slight increase of 0.023 \AA when compared to that of the single crystal, whereas the *b*-axis increased more substantially by $\sim 0.192 \text{ \AA}$. However, the α angle increased by $\sim 6.004^\circ$, and the β angle showed a small decrease of $\sim 0.475^\circ$. It should be noted that for the current analysis, differences below 0.01 \AA and 0.01° were not significant. The differences in the unit cells between single crystal and thin film could be explained by thermal expansion as the thin film was deposited and measured at 300 K, which was much higher than the temperature of single-crystal data collection (113 K). Fig. 3(c) shows the GIWAXS in-plane line scan plots of the same thin film. The pronounced Bragg peak at $q_{xy} = 1.34 \text{ \AA}^{-1}$ was assigned to the (-110) plane. The coherent in-plane island sizes (S_{\parallel}) of the thin films were determined from the full width at half-maximum (FWHM) of the Bragg reflections, based on the Scherrer formula, by $S_{\parallel} = 2\pi 0.94/\text{FWHM}$. For ADT, the averaged $S_{\parallel\text{ADT}}$ based on the pronounced peaks was $S_{\parallel\text{ADT}} = 22.68 \pm 2.09 \text{ nm}$, which was somewhat similar to that of difluoroanthrodithiophene (diF-ADT) under the same growth conditions.³⁸

Fig. 3(b) shows the reciprocal space map of the 30 nm thick β -MT-ADT thin film, which exhibits a ring-like diffraction pattern. These ring-like features indicate that the crystalline islands did not have a well-defined out-of-plane uniaxial orientation. The diffraction peaks can be essentially fitted with the single crystal structure of β -MT-ADT, in which the three axes, *a*, *b*, and *c*, were all slightly increased, whereas the three angles, α , β , and γ , remained essentially unchanged. This suggested that the enlargement of the unit cell parameters resulted from the thermal expansion. In the GIWAXS line scan plots (Fig. 3(d)) the

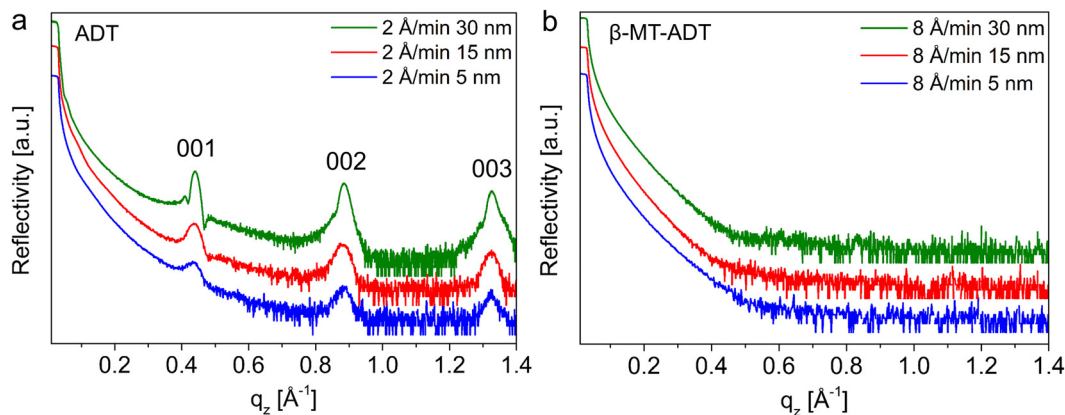


Fig. 2. The XRR plots (reflectivity in logarithmic scales) of (a) ADT and (b) β -MT-ADT thin films with 5, 15, and 30 nm thicknesses. The plots are offset for clarity.

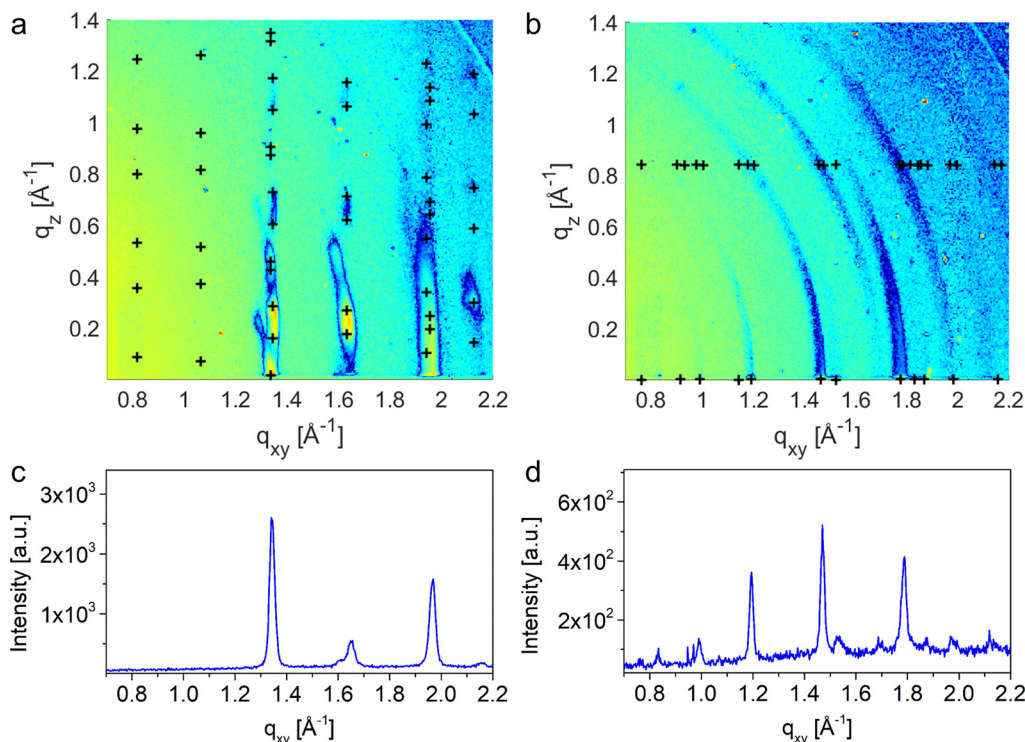


Fig. 3 Reciprocal space maps and GIWAXS line scan plots along the q_{xy} (incidence angle = 0.08°) direction of ADT (a and c) and β -MT-ADT (b and d) thin films with 30 nm thicknesses. The black crosses in (a) and (b) are the simulated diffraction positions based on the single-crystal structure, and the plots in (c) and (d) were obtained by integration of the corresponding 2D images along the q_z direction in the range of $0\text{--}0.15\text{ \AA}^{-1}$.

Table 1 The unit cell parameters of the single crystals and the thin films

Materials	Phase	a (\AA)	b (\AA)	c (\AA)	α ($^\circ$)	β ($^\circ$)	γ ($^\circ$)	V (\AA^3)
ADT	Single crystal (<i>syn</i> -ADT, 113 K)	5.887	7.508	14.347	90.106	94.285	90.414	628.636
	Thin film (<i>syn-anti</i> ADT) (300 K)	5.91	7.70	14.25	96.11	93.81	90.42	643
β -MT-ADT	Single crystal (90 K)	7.455	16.265	6.769	90	90.98	90	820.594
	Thin film (300 K)	7.46	16.49	6.87	90	90.98	90	845

Bragg peaks could be indexed as the $(0k1)$ diffraction peaks. Based on the pronounced Bragg peaks, the average $S_{\parallel\beta\text{-MT-ADT}}$ was determined to be 31.54 ± 3.36 nm.

Morphologies of the thin films

The topographic morphologies of the ADT and β -MT-ADT thin films with nominal thicknesses of 5, 15, and 30 nm were characterized by AFM analysis. Fig. 4 shows representative AFM images of the films. For a 5 nm nominal thickness, ADT could only form islands, which were not fully connected to cover the substrate. As the thicknesses increased to 15 and 30 nm, thin films with wedding-cake like morphologies were formed. The step height of the terraces in the thin films was ~ 1.5 nm, which was consistent with the lattice spacing determined by XRR, *i.e.*, 14.28 \AA , and the molecular length of 13.77 \AA , confirming the uniaxial growth of ADT. Even with the higher growth rate of 8 \AA min^{-1} , β -MT-ADT formed only isolated islands at a low film thickness (5 nm).

As more molecules were deposited, the size of the islands increased, but they could not coalesce with each other to fully cover the substrate when the nominal thickness reached 30 nm.

To obtain an insight into the mode of growth of ADT and β -MT-ADT, the AFM images were quantitatively analyzed based on height–height correlation functions (HHCF).³⁹ For each sample, the HHCFs of several AFM scans were fitted by the function $f(x) = 2\sigma^2[1 - \exp(-(x/\xi)^{2\alpha})]$, where α is the Hurst parameter, ξ is the lateral correlation coefficient, and σ is the root-mean-squared (RMS) roughness. The α values for ADT and β -MT-ADT thin films were extracted by fitting the linear part (on a log scale) of the HHCF curves, and the values used in the HHCF fitting function were averaged for all the AFM images. For ADT, α_{ADT} was 0.63, and for β -MT-ADT, $\alpha_{\beta\text{-MT-ADT}}$ was 0.73. The relatively larger α suggested there was a steeper roughening trend of β -MT-ADT during growth. The ξ for ADT thin films with 5, 15, and 30 nm nominal thicknesses were: $\xi_{\text{ADT},5\text{nm}} = 182.61 \pm 16.13$ nm, $\xi_{\text{ADT},15\text{nm}} = 171.65 \pm 6.00$ nm, and $\xi_{\text{ADT},30\text{nm}} = 180.78 \pm 6.84$ nm. In contrast, to the β -MT-ADT

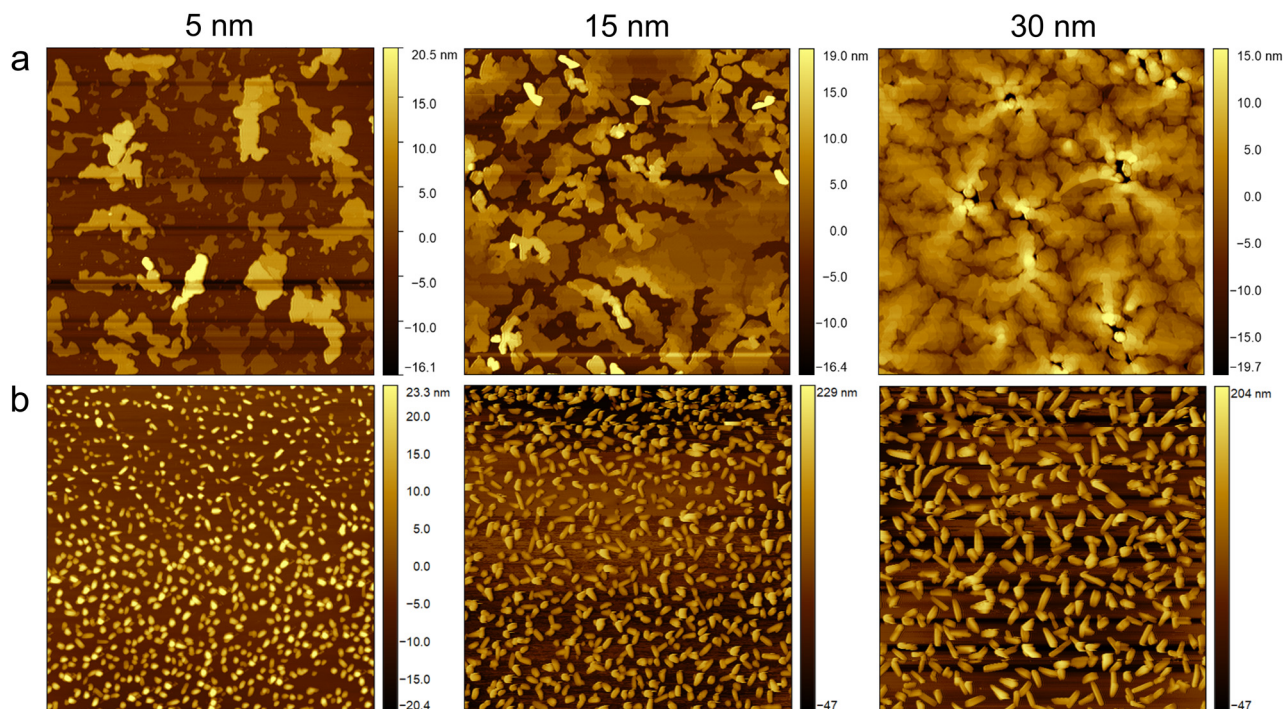


Fig. 4 The AFM images ($7 \times 7 \mu\text{m}$) of ADT (a, upper row) and β -MT-ADT (b, bottom row) thin films with 5, 15, and 30 nm thicknesses.

values, the ζ for the corresponding nominal thicknesses were $\zeta_{\beta\text{-MT-ADT}, 5\text{nm}} = 47.62 \pm 11.07 \text{ nm}$, $\zeta_{\beta\text{-MT-ADT}, 15\text{nm}} = 63.50 \pm 4.57 \text{ nm}$, and $\zeta_{\beta\text{-MT-ADT}, 30 \text{ nm}} = 77.13 \pm 2.98 \text{ nm}$. The ζ values of the ADT thin films in each nominal thickness were ~ 2 – 4 times larger than those of the β -MT-ADT thin films, which indicated their statistically relevant larger surface island sizes. The σ values for the ADT thin films were obtained by eliminating the large crystallites in the images, which might result from the de-wetting of the thin films. For ADT, σ values were: $\sigma_{\text{ADT}, 5\text{nm}} = 5.63 \pm 0.59 \text{ nm}$, $\sigma_{\text{ADT}, 15\text{nm}} = 6.73 \pm 0.67 \text{ nm}$, and $\sigma_{\text{ADT}, 30\text{nm}} = 5.55 \pm 0.37 \text{ nm}$. For the β -MT-ADT the σ values were: $\sigma_{\beta\text{-MT-ADT}, 5\text{nm}} = 7.75 \pm 0.55 \text{ nm}$, $\sigma_{\beta\text{-MT-ADT}, 15\text{nm}} = 18.68 \pm$

0.89 nm , and $\sigma_{\beta\text{-MT-ADT}, 30\text{nm}} = 25.10 \pm 1.19 \text{ nm}$. The β -MT-ADT thin films all exhibited ~ 1.5 – 5 times larger σ values than the corresponding ADT thin films, which suggested their increased large surface area roughness.

Based on the dynamic scaling framework, the ζ and the film thickness D can be fitted to a power-law dependence with $\zeta \sim D^{1/z}$, where $1/z$ refers to the dynamic exponent. Fig. 5(a) shows the log-log scaled ζ and D data for ADT and β -MT-ADT thin films. For ADT, ζ and D could be roughly fitted in a linear regression with $1/z_{\text{ADT}} = 0.02 \pm 0.05$. The large standard error made further interpretation of the linear regression difficult, which might be because of the unreasonable ζ value induced by

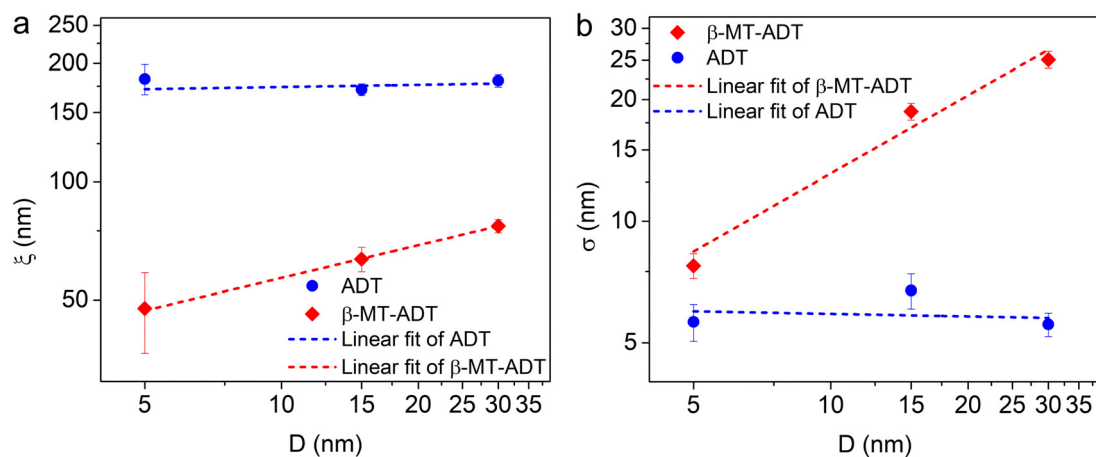


Fig. 5 (a) ζ and (b) σ values extracted from the HHCFs of the AFM images plotted in logarithmic scales. The dashed lines through the data sets are linear regressions used to obtain the scaling coefficients of $1/z$ and β , respectively.

the de-wetting behavior of 5 nm thick film. For β -MT-ADT, a clear dependence between ζ and D could be observed, and the dynamic exponent $1/z_{\beta\text{-MT-ADT}}$ was 0.28 ± 0.01 . This value was ~ 2 – 3 times smaller than that for other well studied organic semiconductors (for DIP, $1/z_{\text{DIP}} = 0.92 \pm 0.20$,⁴⁰ and for diF-ADT, $1/z_{\text{diF-ADT}} = 0.70 \pm 0.16$ ³⁸). Because in all the conditions, no island coalescence occurred for the β -MT-ADT thin films, $1/z_{\beta\text{-MT-ADT}}$ mainly describes the lateral growth speed of the isolated islands.

The power-law dependence of σ and the film thickness D , $\sigma \sim D^\beta$, where β represents the growth exponent, was also investigated for the ADT and β -MT-ADT thin films. As shown in Fig. 5(b), the fit for σ and D of ADT thin films yielded a β ($\beta_{\text{ADT}} = -0.02 \pm 0.11$) close to zero. The irregular evolution of roughness might be due to the de-wetting behavior of the relatively thinner films or it might indicate that the growth of ADT was probably more complex than a simple roughening process described by a power law.⁴¹ For β -MT-ADT, a clear power law for the σ and D could be observed with $\beta_{\beta\text{-MT-ADT}} = 0.64 \pm 0.12$. This value was larger than those of the widely studied materials pentacene ($\beta = 0.27 \pm 0.03$)⁴² and *para*-sexiphenyl (6P) ($\beta_{6\text{P}} = 0.49$),¹⁶ which showed terraced mounds in growth. However, it was smaller than that of DIP with $\beta = 0.748 \pm 0.05$ ⁴⁰ and $\beta = 0.772 \pm 0.031$,⁴³ which could be termed unusually rapid roughness evolution. The relatively large β value indicated a net

uphill transport of molecules for β -MT-ADT during growth, because for comparison $\beta = 0.5$ would correspond to a growth scenario without interlayer transport.

Combining the XRR, GIWAXS, and AFM analyses, ADT can be seen to grow in a similar way to other prototypical rod-like organic semiconductors, which have a uniaxial upright orientation, wedding-cake morphology, and fast island coalescence. However, the domains in the β -MT-ADT thin films had a broad orientation distribution, no apparent island morphology, and slow island coalescence. In addition, ADT thin films show a considerably larger lateral correlation length, a smaller coherent domain size, and reduced roughness compared to the β -MT-ADT thin films. All the information indicated that the parent ADT had a larger diffusion length, and the diffusion in the lateral direction was preferred when compared to β -MT-ADT. As ADT and β -MT-ADT have the same molecular backbone, these differences most likely originated from the substitution of the methylthio groups at the β -positions. Based on the theoretical calculation and the single crystal structure, the two β -methylthio groups seemed to be fixed in the same plane with the molecular backbone.³¹ Nevertheless, they could possibly vibrate along the S–C single bonds in the gas phase. This type of vibration was likely to favor molecular desorption and diffusion, and might contribute to overcoming the step-edge energy barriers between neighboring molecular layers,

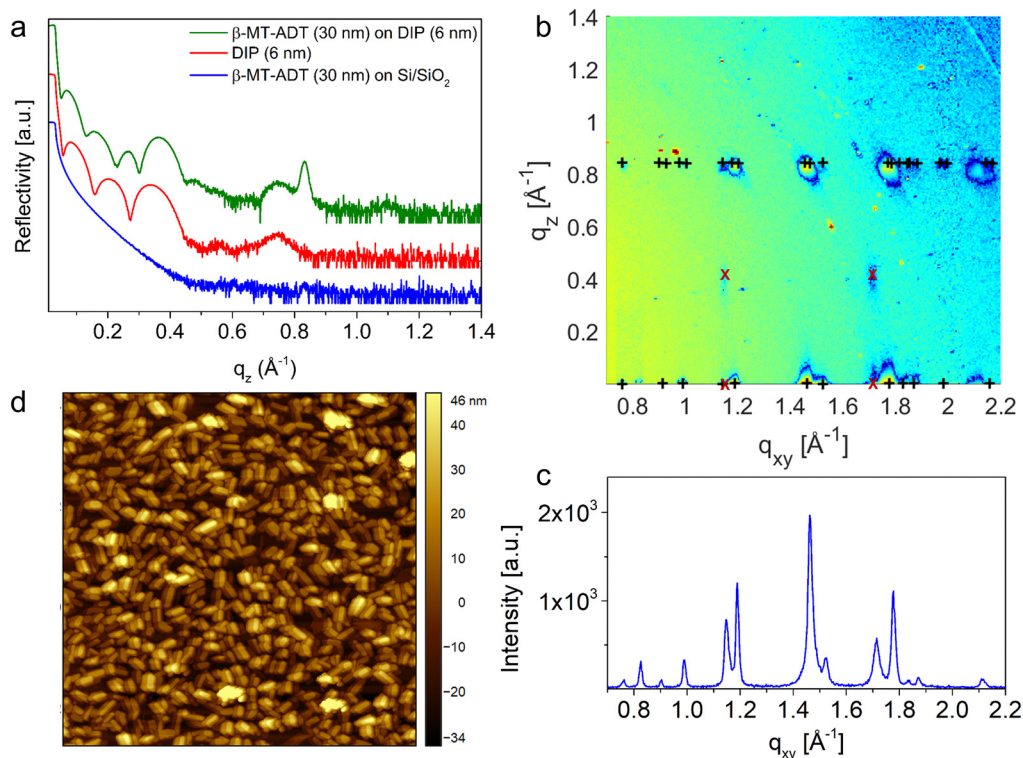


Fig. 6 (a) The XRR plots of β -MT-ADT thin film (30 nm), DIP (6 nm), and β -MT-ADT (30 nm) on DIP (6 nm), and the black crosses mark the simulated diffraction positions of β -MT-ADT based on its single-crystal structure, and the red crosses label the diffractions of the DIP layer. (c) The GIWAXS line scan (incidence angle = 0.08°) plot of β -MT-ADT (30 nm) on DIP (6 nm), and the plot is obtained by integration of the corresponding 2D image along the q_z direction in the range of 0 – 0.15 \AA^{-1} . (d) The AFM image ($7 \times 7 \text{ \mu m}$) of β -MT-ADT (30 nm) on DIP (6 nm).

leading to strong roughening.^{16,44–48} Therefore, it was concluded that modifying the ADT molecular backbone with methylthio groups at the β -positions substantially changed the thin film growth behavior.

Templating the growth of β -MT-ADT

From the previous analysis, β -MT-ADT did not seem to grow as a continuous thin film on bare Si/SiO₂ substrate. However, a previous study reported that β -MT-ADT grown on an ODTs-modified Si/SiO₂ substrate showed a relatively good performance in thin film OFETs.³¹ Hence, good quality thin films of β -MT-ADT could be formed under these conditions.³¹ To investigate how the surface treatment of the substrate influenced the growth of β -MT-ADT, growing β -MT-ADT on DIP, which is widely applied as a templating layer for thin film growth of organic semiconductors, was carried out.^{49,50} The substrate temperature used for the DIP thin film growth was 393 K, and the thickness was tuned to 6 nm, because under these conditions, DIP could grow in a layer-by-layer mode and form a smooth thin film with high crystallinity.^{49,51}

Fig. 6(a) shows the XRR curve (red color) of the 6 nm thick DIP film. Clear Kiessig fringes were present, which show the high smoothness of the film. In addition, a broad Bragg peak with q_z at 0.725 Å⁻¹ can also be observed, which corresponded to the (002) planes of the DIP high-temperature phase.^{49,51} After deposition of β -MT-ADT with a nominal thickness of 30 nm on the top of DIP, a new pronounced Bragg peak with q_z at 0.840 Å⁻¹ was visible, which is ascribed to the (100) reflection based on the single-crystal structure of β -MT-ADT. This contrasts sharply with the XRR data of β -MT-ADT grown on bare Si/SiO₂, where no diffraction characteristics were observed. This suggests that the crystal quality of the β -MT-ADT thin film is improved by the addition of a DIP templating layer.

Ring-like diffraction features disappeared in the reciprocal space map (Fig. 6(b)). Instead, well-defined diffraction spots were observed, which matched well with the single crystal structure of β -MT-ADT. The average coherent island size was determined to be $S_{\parallel\beta\text{-MT-ADT/DIP}} = 33.07 \pm 7.85$ nm based on the GIWAXS line scan plot (Fig. 6(c)). In the AFM image (Fig. 6(d)), the crystallites showed a more regular shape and coalesced with their neighbors. The RMS roughness of the film was 16.02 nm, which was much smoother than that grown without DIP.

Combining all the information extracted from XRR, GIWAXS reciprocal space maps, and AFM image analysis, the templating layer uniaxially aligned the crystalline islands' orientation, and increased the molecular diffusion length in the lateral direction. Thus, it significantly improved the quality of the thin films.

Conclusions

In conclusion, the thin film growth behavior of ADT (with a mixture of *syn*- and *anti*-isomers) and its β -methylthiolated derivative β -MT-ADT was studied on Si/SiO₂ substrates. The XRD analysis, especially the synchrotron-based GIWAXS data,

indicates that the ADT grows uniaxially upright-oriented on the substrate in a similar way to the *syn*-isomer structure. At the same time, the crystalline islands of β -MT-ADT have a wide orientational distribution, even though the crystal structure is basically maintained in the thin film. Qualitative and quantitative analysis of the AFM images of the two sets of thin films with different thicknesses suggests that ADT forms a wedding-cake-like morphology, similar to other prototypical organic semiconductors. In contrast, β -MT-ADT forms only isolated islands with a high roughness, and the islands do not coalesce up to a thickness of 30 nm. The analysis implies that the minor modification of the ADT molecular backbone at the β -positions with methylthio groups substantially impacts the thin film growth behavior. When a DIP templating layer is deposited beforehand, the islands of β -MT-ADT become uniaxially oriented, and the crystal quality of the thin film is significantly improved. This kind of templating is similar to the growth of rubrene on a pentacene templating layer^{52,53} or a C₆₀ growth on a DIP templating layer.²⁹

This paper not only reports the thin film growth behavior of two representative materials in a solid-state structure, but also reveals how the molecular modification could significantly affect the thin film growth behavior, providing guidance for future material design for developing high-performance organic semiconductors based on a thin film structure design.

Conflicts of interest

There are no conflicts to declare.

Acknowledgements

We acknowledge the European Synchrotron Radiation Facility (ESRF) for providing synchrotron radiation facilities and, in particular, use of the ID10 beamline. CW thanks the Alexander-von-Humboldt Foundation for the postdoctoral fellowship. GD gratefully acknowledges support by the German Ministry of Economy (BMW). FS acknowledges financial support from the DFG.

References

- 1 S. R. Forrest, Ultrathin Organic Films Grown by Organic Molecular Beam Deposition and Related Techniques, *Chem. Rev.*, 1997, **97**, 1793–1896.
- 2 S. R. Forrest, The path to ubiquitous and low-cost organic electronic appliances on plastic, *Nature*, 2004, **428**, 911–918.
- 3 H. Uoyama, K. Goushi, K. Shizu, H. Nomura and C. Adachi, Highly efficient organic light-emitting diodes from delayed fluorescence, *Nature*, 2012, **492**, 234–238.
- 4 H. Sirringhaus, 25th Anniversary Article: Organic Field-Effect Transistors: The Path Beyond Amorphous Silicon, *Adv. Mater.*, 2014, **26**, 1319–1335.

- 5 N. E. Jackson, B. M. Savoie, T. J. Marks, L. X. Chen and M. A. Ratner, The Next Breakthrough for Organic Photovoltaics?, *J. Phys. Chem. Lett.*, 2015, **6**, 77–84.
- 6 Q. Li, Y. Guo and Y. Liu, Exploration of Near-Infrared Organic Photodetectors, *Chem. Mater.*, 2019, **31**, 6359–6379.
- 7 U. Heinemeyer, K. Broch, A. Hinderhofer, M. Kytka, R. Scholz, A. Gerlach and F. Schreiber, Real-Time Changes in the Optical Spectrum of Organic Semiconducting Films and Their Thickness Regimes during Growth, *Phys. Rev. Lett.*, 2010, **104**, 257401.
- 8 J. Wagner, M. Gruber, A. Hinderhofer, A. Wilke, B. Bröker, J. Frisch, P. Amsalem, A. Vollmer, A. Opitz, N. Koch, F. Schreiber and W. Brütting, High Fill Factor and Open Circuit Voltage in Organic Photovoltaic Cells with Diindenoperylene as Donor Material, *Adv. Funct. Mater.*, 2010, **20**, 4295–4303.
- 9 C. A. W. Brütting, *Physics of Organic Semiconductors*, Wiley-VCH, 2nd edn, 2012.
- 10 Y. Wen, Y. Liu, Y. Guo, G. Yu and W. Hu, Experimental Techniques for the Fabrication and Characterization of Organic Thin Films for Field-Effect Transistors, *Chem. Rev.*, 2011, **111**, 3358–3406.
- 11 U. Hörmann, C. Lorch, A. Hinderhofer, A. Gerlach, M. Gruber, J. Kraus, B. Sykora, S. Grob, T. Linderl, A. Wilke, A. Opitz, R. Hansson, A. S. Anselmo, Y. Ozawa, Y. Nakayama, H. Ishii, N. Koch, E. Moons, F. Schreiber and W. Brütting, Voc from a Morphology Point of View: the Influence of Molecular Orientation on the Open Circuit Voltage of Organic Planar Heterojunction Solar Cells, *J. Phys. Chem. C*, 2014, **118**, 26462–26470.
- 12 F. Liscio, C. Albonetti, K. Broch, A. Shehu, S. D. Quiroga, L. Ferlauto, C. Frank, S. Kowarik, R. Nervo, A. Gerlach, S. Milita, F. Schreiber and F. Biscarini, Molecular Reorganization in Organic Field-Effect Transistors and Its Effect on Two-Dimensional Charge Transport Pathways, *ACS Nano*, 2013, **7**, 1257–1264.
- 13 R. Ruiz, D. Choudhary, B. Nickel, T. Toccoli, K.-C. Chang, A. C. Mayer, P. Clancy, J. M. Blakely, R. L. Headrick, S. Iannotta and G. G. Malliaras, Pentacene Thin Film Growth, *Chem. Mater.*, 2004, **16**, 4497–4508.
- 14 A. C. Dürr, F. Schreiber, K. A. Ritley, V. Kruppa, J. Krug, H. Dosch and B. Struth, Rapid Roughening in Thin Film Growth of an Organic Semiconductor (Diindenoperylene), *Phys. Rev. Lett.*, 2003, **90**, 016104.
- 15 M. Klopotek, H. Hansen-Goos, M. Dixit, T. Schilling, F. Schreiber and M. Oettel, Monolayers of hard rods on planar substrates. II. Growth, *J. Chem. 2f Step-Edge Barriers in Organic Thin-Film Growth*, *Science*, 2008, **321**, 108–111.
- 16 G. Hlawacek, P. Puschnig, P. Frank, A. Winkler, C. Ambrosch-Draxl and C. Teichert, Characterization of Step-Edge Barriers in Organic Thin-Film Growth, *Science*, 2008, **321**, 108–111.
- 17 S. Yim and T. S. Jones, Anomalous scaling behavior and surface roughening in molecular thin-film deposition, *Phys. Rev. B: Condens. Matter Mater. Phys.*, 2006, **73**, 161305.
- 18 S. Bommel, N. Kleppmann, C. Weber, H. Spranger, P. Schäfer, J. Novak, S. V. Roth, F. Schreiber, S. H. L. Klapp and S. Kowarik, Unravelling the multilayer growth of the fullerene C60 in real time, *Nat. Commun.*, 2014, **5**, 5388.
- 19 W. Janke and T. Speck, Multiscale modeling of structure formation of C60 on insulating CaF2 substrates, *J. Chem. Phys.*, 2021, **154**, 234701.
- 20 G. Witte and C. Wöll, Growth of aromatic molecules on solid substrates for applications in organic electronics, *J. Mater. Res.*, 2004, **19**, 1889–1916.
- 21 V. Belova, P. Beyer, E. Meister, T. Linderl, M.-U. Halbach, M. Gerhard, S. Schmidt, T. Zechel, T. Meisel, A. V. Generalov, A. S. Anselmo, R. Scholz, O. Konovalov, A. Gerlach, M. Koch, A. Hinderhofer, A. Opitz, W. Brütting and F. Schreiber, Evidence for Anisotropic Electronic Coupling of Charge Transfer States in Weakly Interacting Organic Semiconductor Mixtures, *J. Am. Chem. Soc.*, 2017, **139**, 8474–8486.
- 22 L. Jiang, J. Liu, X. Lu, L. Fu, Y. Shi, J. Zhang, X. Zhang, H. Geng, Y. Hu, H. Dong, L. Jiang, J. Yu and W. Hu, Controllable growth of C8-BTBT single crystalline micro-ribbon arrays by a limited solvent vapor-assisted crystallization (LSVC) method, *J. Mater. Chem. C*, 2018, **6**, 2419–2423.
- 23 H. Spreitzer, B. Kaufmann, C. Ruzié, C. Röthel, T. Arnold, Y. H. Geerts, C. Teichert, R. Resel and A. O. F. Jones, Alkyl chain assisted thin film growth of 2,7-dioctyloxy-benzothienobenzothiophene, *J. Mater. Chem. C*, 2019, **7**, 8477–8484.
- 24 J. Weszka, P. Jarka, D. PakvBa, L. A. DobrzaDski, M. DombDski and J. Jurusik, Studying of kinetic growth of organic thin films, *J. Achiev. Mater. Manuf. Eng.*, 2009, **35**, 29–36.
- 25 F. Schreiber, Structure and growth of self-assembling monolayers, *Prog. Surf. Sci.*, 2000, **65**, 151–257.
- 26 M. C. Gerstenberg, F. Schreiber, T. Y. B. Leung, G. Bracco, S. R. Forrest and G. Scoles, Organic semiconducting thin film growth on an organic substrate: \$3,4,9,10\$-perylene-tetracarboxylic dianhydride on a monolayer of decanethiol self-assembled on Au(111), *Phys. Rev. B: Condens. Matter Mater. Phys.*, 2000, **61**, 7678–7685.
- 27 A. Hinderhofer and F. Schreiber, Organic–Organic Heterostructures: Concepts and Applications, *Chem. Phys. Chem.*, 2012, **13**, 628–643.
- 28 P. Sullivan, T. S. Jones, A. J. Ferguson and S. Heutz, Structural templating as a route to improved photovoltaic performance in copper phthalocyanine/fullerene (C60) heterojunctions, *Appl. Phys. Lett.*, 2007, **91**, 233114.
- 29 A. Hinderhofer, A. Gerlach, K. Broch, T. Hosokai, K. Yonezawa, K. Kato, S. Kera, N. Ueno and F. Schreiber, Geometric and Electronic Structure of Templated C60 on Diindenoperylene Thin Films, *J. Phys. Chem. C*, 2013, **117**, 1053–1058.
- 30 M. Mamada, H. Katagiri, M. Mizukami, K. Honda, T. Minamiki, R. Teraoka, T. Uemura and S. Tokito, syn-/anti-Anthradithiophene Derivative Isomer Effects on Semiconducting Properties, *ACS Appl. Mater. Interfaces*, 2013, **5**, 9670–9677.
- 31 C. Wang, D. Hashizume, M. Nakano, T. Ogaki, H. Takenaka, K. Kawabata and K. Takimiya, “Disrupt and induce” intermolecular interactions to rationally design organic semiconductor crystals: from herringbone to rubrene-like pitched π -stacking, *Chem. Sci.*, 2020, **11**, 1573–1580.

- 32 M. M. Payne, S. R. Parkin, J. E. Anthony, C.-C. Kuo and T. N. Jackson, Organic Field-Effect Transistors from Solution-Deposited Functionalized Acenes with Mobilities as High as $1 \text{ cm}^2/\text{V}\cdot\text{s}$, *J. Am. Chem. Soc.*, 2005, **127**, 4986–4987.
- 33 O. D. Jurchescu, S. Subramanian, R. J. Kline, S. D. Hudson, J. E. Anthony, T. N. Jackson and D. J. Gundlach, Organic Single-Crystal Field-Effect Transistors of a Soluble Anthradithiophene, *Chem. Mater.*, 2008, **20**, 6733–6737.
- 34 R. K. Hallani, K. J. Thorley, Y. Mei, S. R. Parkin, O. D. Jurchescu and J. E. Anthony, Structural and Electronic Properties of Crystalline, Isomerically Pure Anthradithiophene Derivatives, *Adv. Funct. Mater.*, 2016, **26**, 2341–2348.
- 35 V. Podzorov, E. Menard, A. Borissov, V. Kiryukhin, J. A. Rogers and M. E. Gershenson, Intrinsic Charge Transport on the Surface of Organic Semiconductors, *Phys. Rev. Lett.*, 2004, **93**, 086602.
- 36 C. Sundar Vikram, J. Zaumseil, V. Podzorov, E. Menard, L. Willett Robert, T. Someya, E. Gershenson Michael and A. Rogers John, Elastomeric Transistor Stamps: Reversible Probing of Charge Transport in Organic Crystals, *Science*, 2004, **303**, 1644–1646.
- 37 F. Schreiber, Organic molecular beam deposition: Growth studies beyond the first monolayer, *Phys. Status Solidi*, 2004, **201**, 1037–1054.
- 38 T. Storzer, A. Hinderhofer, C. Zeiser, J. Novák, Z. Fišer, V. Belova, B. Reisz, S. Maiti, G. Duva, R. K. Hallani, A. Gerlach, J. E. Anthony and F. Schreiber, Growth, Structure, and Anisotropic Optical Properties of Difluoro-anthradithiophene Thin Films, *J. Phys. Chem. C*, 2017, **121**, 21011–21017.
- 39 J. Krug, Origins of scale invariance in growth processes, *Adv. Phys.*, 1997, **46**, 139–282.
- 40 A. C. Dürr, F. Schreiber, K. A. Ritley, V. Kruppa, J. Krug, H. Dosch and B. Struth, Rapid Roughening in Thin Film Growth of an Organic Semiconductor (Diindenoperylene), *Phys. Rev. Lett.*, 2003, **90**, 016104.
- 41 E. Empting, M. Klopotek, A. Hinderhofer, F. Schreiber and M. Oettel, Lattice gas study of thin-film growth scenarios and transitions between them: Role of substrate, *Phys. Rev. E*, 2021, **103**, 023302.
- 42 S. Zorba, Y. Shapir and Y. Gao, Fractal-mound growth of pentacene thin films, *Phys. Rev. B: Condens. Matter Mater. Phys.*, 2006, **74**, 245410.
- 43 X. N. Zhang, E. Barrena, D. G. de Oteyza and H. Dosch, Transition from layer-by-layer to rapid roughening in the growth of DIP on SiO_2 , *Surf. Sci.*, 2007, **601**, 2420–2425.
- 44 M. B. Casu, S.-A. Savu, P. Hoffmann, B.-E. Schuster, T. O. Menteş, M. A. Niño, A. Locatelli and T. Chassé, Direct observation of step-edge barrier effects and general aspects of growth processes: morphology and structure in diindenoperylene thin films deposited on Au(100) single crystals, *CrystEngComm*, 2011, **13**, 4139–4144.
- 45 K. Palczynski, P. Herrmann, G. Heimel and J. Dzubielia, Characterization of step-edge barrier crossing of para-sexiphenyl on the ZnO (100) surface, *Phys. Chem. Chem. Phys.*, 2016, **18**, 25329–25341.
- 46 F.-J. Meyer Zu Heringdorf, M. C. Reuter and R. M. Tromp, Growth dynamics of pentacene thin films, *Nature*, 2001, **412**, 517–520.
- 47 C. Frank, J. Novák, R. Banerjee, A. Gerlach, F. Schreiber, A. Vorobiev and S. Kowarik, Island size evolution and molecular diffusion during growth of organic thin films followed by time-resolved specular and off-specular scattering, *Phys. Rev. B: Condens. Matter Mater. Phys.*, 2014, **90**, 045410.
- 48 T. B. T. To, V. B. de Sousa and F. D. A. Aarão Reis, Thin film growth models with long surface diffusion lengths, *Physica A*, 2018, **511**, 240–250.
- 49 S. Kowarik, A. Gerlach, S. Sellner, F. Schreiber, L. Cavalcanti and O. Konovalov, Real-Time Observation of Structural and Orientational Transitions during Growth of Organic Thin Films, *Phys. Rev. Lett.*, 2006, **96**, 125504.
- 50 R. Scholz, L. Gisslén, B. E. Schuster, M. B. Casu, T. Chassé, U. Heinemeyer and F. Schreiber, Resonant Raman spectra of diindenoperylene thin films, *J. Chem. Phys.*, 2011, **134**, 014504.
- 51 X. Zhang, E. Barrena, D. Goswami, D. G. de Oteyza, C. Weis and H. Dosch, Evidence for a Layer-Dependent Ehrlich-Schwöbel Barrier in Organic Thin Film Growth, *Phys. Rev. Lett.*, 2009, **103**, 136101.
- 52 M. A. Fusella, S. Yang, K. Abbasi, H. H. Choi, Z. Yao, V. Podzorov, A. Avishai and B. P. Rand, Use of an Underlayer for Large Area Crystallization of Rubrene Thin Films, *Chem. Mater.*, 2017, **29**, 6666–6673.
- 53 M. Haemori, J. Yamaguchi, S. Yaginuma, K. Itaka and H. Koinuma, Fabrication of Highly Oriented Rubrene Thin Films by the Use of Atomically Finished Substrate and Pentacene Buffer Layer, *Jpn. J. Appl. Phys.*, 2005, **44**, 3740–3742.